Effect of Micro-bubbles on a Turbulent Boundary Layer

H. L. Cao, W. Guo, X. H. Li and Y. Zhou

Abstract Micro-bubble is one of the most promising methods for reduction of skin friction drag. The injection of gas bubbles into a turbulent boundary layer may have multiple impacts on the turbulent flow structure. This work aims to understand the interaction between micro-bubbles and the turbulent boundary layer, especially the effect of the bubble layer thickness on the skin-friction drag reduction. Large eddy simulation was conducted for a turbulent boundary layer over a flat plate, injected with micro-bubbles, with a view to reduce skin-friction drag. The Reynolds number Re_θ examined was 1430 based on the momentum thickness θ and free-stream velocity U_∞. A three-dimensional perturbation method was deployed to generate a turbulent boundary layer within a short distance of inflow.

Keywords Large-eddy simulation · Microbubble drag reduction
Boundary layer

1 Introduction

The use of micro-bubble as a way to reduce skin friction in turbulent flows has been a focus for researchers in the expectation that which is applicable to ships. Previous experimental work has shown it can reduce the skin friction by as much as 80% [5, 7]. Ferrante and Elghobashi [2, 3] reported their direct numerical simulation study to explain the mechanisms of drag reduction in a microbubble-laden spatially developing turbulent boundary layer, and also the Reynolds effect on drag reduction. Our objective in the present paper is to further explain the interaction between micro-bubbles and the turbulent boundary layer, especially the effect of the micro-bubble layer thickness on the skin-friction drag reduction.

H. L. Cao (✉) · W. Guo · X. H. Li · Y. Zhou
Shenzhen Graduate School, Harbin Institute of Technology, Shenzhen, China
e-mail: caohualilmy@163.com

2 Simulation Method

It is well understood that the inner layer of the turbulent boundary layer has low speed streaks, while the outer layer has large scale coherent structures. In order to reproduce turbulent flow numerically, here we follow Sandham et al. [6] method, in which the streamwise and wall-normal fluctuations were generated with one mode in the inner region and three modes in the outer region. Disturbances in the inner region (denoted as $\hat{u}^{\text{inner}}$) represents lifted streaks, with a peak at a location of $y_{p,j}^+$, while the outer region disturbances (denoted as $\hat{u}^{\text{outer}}$) represent three-dimensional vortices. The disturbances can be written as follows:

$$\hat{u}^{\text{inner}} = c_{1,0}y^+ e^{-y^+/y_{p,0}^+} \sin(\omega_0 t)\, \cos(\beta_0 z + \varphi_0) \tag{1}$$

$$\hat{v}^{\text{inner}} = c_{2,0}(y^+)^2 e^{-(y^+/y_{p,0}^+)^2} \sin(\omega_0 t)\, \cos(\beta_0 z + \varphi_0) \tag{2}$$

$$\hat{u}^{\text{outer}} = \sum_{j=1}^{3} c_{1,j}y/y_{p,j}e^{-y/y_{p,j}} \sin(\omega_j t)\, \cos(\beta_j z + \varphi_j) \tag{3}$$

$$\hat{v}^{\text{outer}} = \sum_{j=1}^{3} c_{2,j}(y/y_{p,j})^2 e^{-(y/y_{p,j})^2} \sin(\omega_j t) \cos(\beta_j z + \varphi_j) \tag{4}$$

where subscripts $j = 0, 1, 2, 3$ are mode indices, y^+ is the y^- coordinate in wall units and the $c_{i,j}$ are constants. Forcing frequencies are denoted by ω_j, spanwise wave numbers by β_j, and phase shiftes by φ_j.

Figure 1 shows a schematic of the turbulent boundary flow over a flat plate. The large-eddy simulation (LES) used presently is applied to a computational domain of $10\delta \times 3\delta \times 3\delta$ (δ is the turbulent boundary thickness) with a grid of $148 \times 90 \times 90$ points, uniformly distributed in the streamwise and spanwise directions and stretched in the wall-normal direction (Fig. 1b). The grid resolution for inflow is approximately $\Delta x^+ = 38$ and $\Delta z^+ = 18$ with 10 points in the viscous sublayer ($y_{\text{min}}^+ = 0.61$). Superscript + denotes normalization by wall units, e.g. $U^+ = U/u_\tau$ and $y^+ = yu_\tau/v$, where U is the streamwise mean velocity, u_τ is the wall friction velocity and v is the kinematic viscosity of fluid. At the lower wall, a no-slip condition was used for the velocity components, and at the upper surface, a free-slip boundary condition was applied. Periodic boundary conditions were used in the spanwise direction.

Figure 2 shows the comparison for the mean streamwise velocity $<U>^+$ and three Reynolds stresses $<u'^2>^+$, $<v'^2>^+$ and $<u'v'>^+$ at $x = 9\delta$, where $Re_\theta = 1430$. In this paper, $<\ >$ represents spatial averaging in the spanwise (z) direction in addition to time averaging of the enclosed quantity. The mean velocity profile is in good agreement with experimental profile obtained by Degraaff and
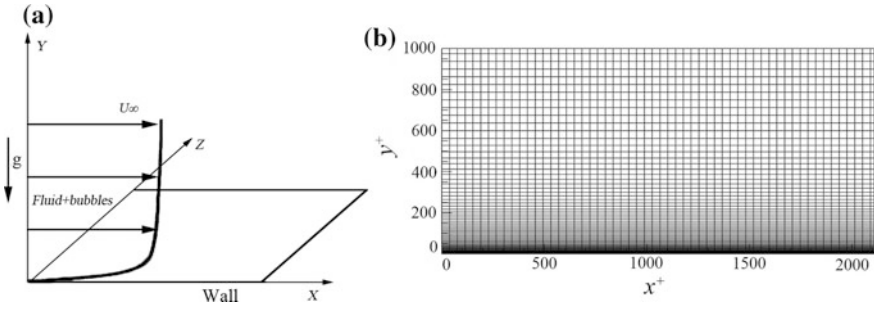
Fig. 1 **a** Schematic of turbulent boundary layer flow over a flat plate **b** typical computational grid
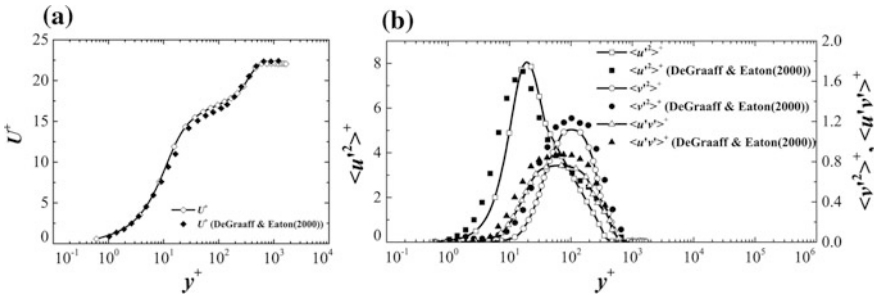

Fig. 2 Comparison between the LES simulation and measurements at $x = 9\delta$: **a** the streamwise mean velocity; **b** Reynolds stresses, at $Re_\theta = 1430$

Eaton at the same Re_θ [1]. The difference in the magnitude of the peak of $<v'^2>^+$ and $<u'v'>^+$ is probably due to experimental uncertainty. Degraaff and Eaton [1] indicate a 10% error in the measured value of $<u'v'>^+$. The results provide a validation for the single-phase simulation.

Then, the micro-bubbles are introduced at the inlet along with the fluid through the wall. The bubbly air-liquid flows are treated by Mixture model. The size of micro-bubble is 40 μm. Two parameters are investigated, i.e. the inlet air volume fraction $\Phi_{v, in}$ and micro-bubble layer thickness h^+ (micro-bubble layer thickness along with y-direction (Fig. 1a)).

3 Results and Discussion

The effect of micro-bubbles may depend on whether the turbulent boundary layer is on the lower or upper side of the plate. This work is focused on the turbulent boundary layer over the lower side. Given $\Phi_{v, in} = 0.1$, the ratio C_f/C_{f0} from calculation and measurement [4] are 0.855 and 0.857, respectively, where C_f and C_{f0}
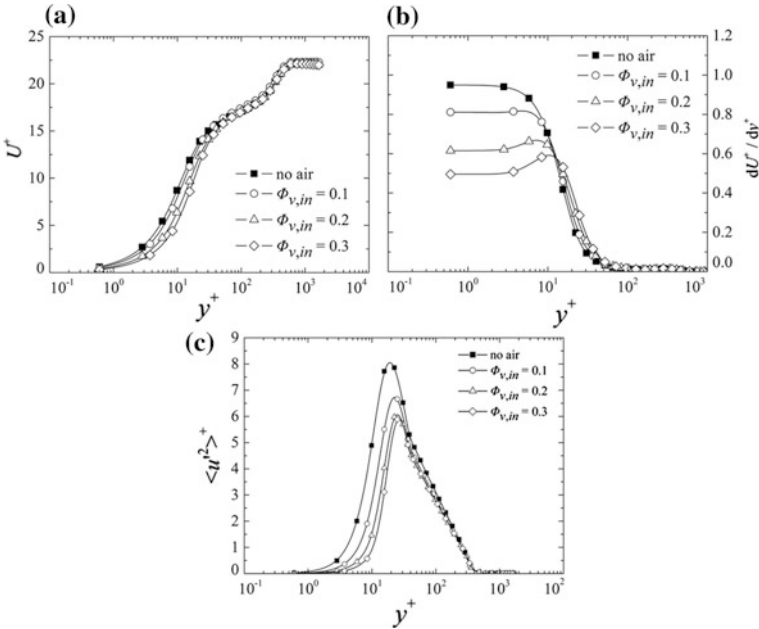
Fig. 3 **a** Mean streamwise velocity; **b** mean streamwise velocity gradient; **c** Reynolds stress at $x = 9\delta$

are the skin-friction coefficients with and without the presence of micro-bubbles. As $\Phi_{v,in}$ increases from 0.1 to 0.3, the average drag reduction increases from 14.5 to 48.6%. Figure 3 shows the profiles of U^+, dU^+/dy^+ and $<u'^2>^+$ for different $\Phi_{v,in}$. The effect of the micro-bubbles is appreciable for $y^+ \leq 10$. The dU^+/dy^+ decreases significantly (Fig. 3b) with the increase in $\Phi_{v,in}$, implying a drag reduction. The viscous layer grows gradually in thickness with an upward shift of the buffer layer, resulting from the rising bubbles which distribute themselves within the boundary layer. There is a marked decrease in $<u'^2>^+$ (Fig. 3c) for $y^+ \leq 20$ and the peak is shifted slightly away from the wall. It has been observed based on the instantaneous vorticity ω_x contours in the (y, z) plane (now shown) that the streamwise vortical structures are dislocated from the wall due to the presence of the micro-bubbles. Furthermore, the spanwise separation between streaky structures is increased.

The effect of h^+ on the drag reduction is investigated, in which five h^+ values are chosen, i.e., 10, 50, 200, 560 and 850. Figure 4 shows profiles of the mean volume fraction and volume fraction gradient of micro-bubble distribution along the vertical direction at $x = 9\delta$. We can find that the concentration of microbubbles at
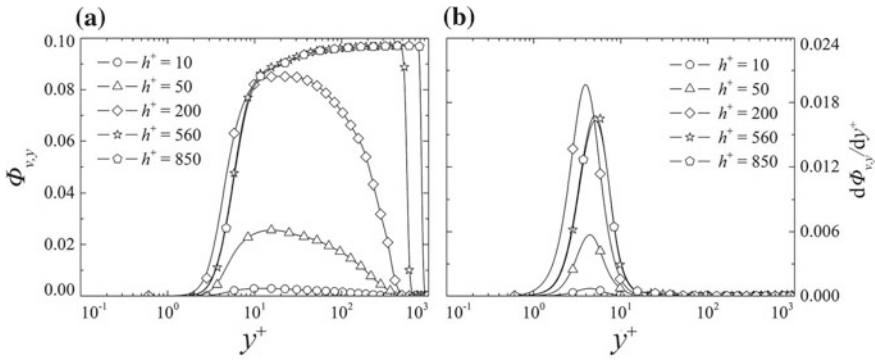
(a) The average volume fraction of micro-bubble; (b) The volume fraction gradient of micro-bubble;

Fig. 4 Profiles of the distribution along the vertical direction at $x = 9\delta$

the near wall region becomes smaller with the increasing of micro-bubble layer thickness h, which is not beneficial to drag reduction. When the micro-bubble was injected into the boundary layer, the large scale vortical structure broke into small scale structure and the vorticity also decreased (Fig. 5a, b). It has been found that, when h^+ is less than 560 (corresponding to the boundary layer thickness), the average volume fraction of bubbles along the x direction decreases and the ability to retain bubbles on the wall is unstable. On the other hand, for $h^+ = 560$ and 850, the thick micro-bubble layer is rather stable; so the bubble layer that is attached to the wall, which is beneficial to drag reduction.
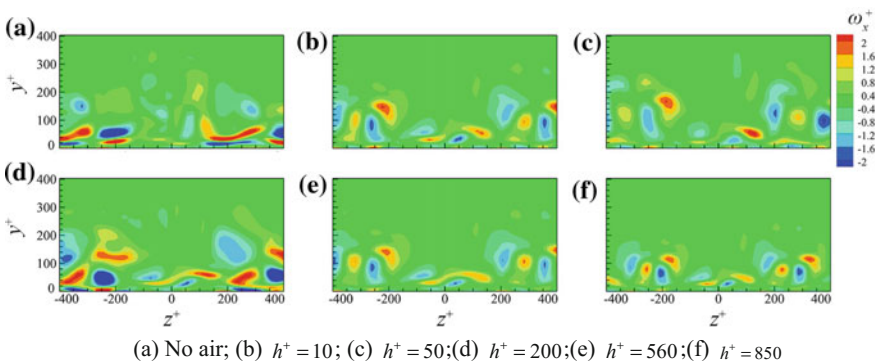
(a) No air; (b) $h^+ = 10$; (c) $h^+ = 50$; (d) $h^+ = 200$; (e) $h^+ = 560$; (f) $h^+ = 850$

Fig. 5 Instantaneous streamwise vorticity at $x = 9\delta$ in y-z plane

4 Conclusion

This study shows that the presence of micro-bubbles acts to decrease the stream-wise mean velocity near the wall and to push away the streamwise vortical structures from the wall, thus producing drag reduction. The drag reduction is strongly dependent on the micro-bubble layer thickness h^+. The result shows that the optimum micro-bubble layer thickness is $h^+ = 560$, which corresponds to the boundary layer thickness.

References

1. Degraaff DB, Eaton JK (2000) Reynolds-number scaling of the flat-plate turbulent boundary layer. J Fluid Mech 422:319–346
2. Ferrante A, Elahobashi S (2004) On the physical mechanisms of drag reduction in a spatially developing turbulent boundary layer laden with microbubbles. J Fluid Mech 503:345–355
3. Ferrante A, Elahobashi S (2005) Reynolds number effect on drag reduction in a microbubble-laden spatially developing turbulent boundary layer. J Fluid Mech 543:93–106
4. Madavan NK, Deutsch S, Merkle CL (1983) Reduction of turbulent skin friction by microbubbles. Tech Memorandum 10:1–38
5. Merkle CL, Deutsch S (1992) Microbubble drag reduction in liquid turbulent boundary layers. Appl Mech Rev 45(3):103–127
6. Sandham ND, Yao YF, Lawal AA (2003) Large-eddy simulation of transonic turbulent flow over a bump. Int J Heat Fluid Flow 24(4):584–595
7. Sanders WC, Winkel EW, Dowling DR, Perlin M, Ceccio SL (2006) Bubble friction drag reduction in a high Reynolds number flat plate turbulent boundary layer. J Fluid Mech 552:353–380